Radiation Physics and Chemistry 176 (2020) 109078

Contents lists available at ScienceDirect

Radiation Physics and Chemistry

journal homepage: www.elsevier.com/locate/radphyschem

Microdosimetry with a 3D silicon on insulator (SOI) detector in a low energy proton beamline

Andreas Tefre Samnøy[a,*], Kristian S. Ytre-Hauge[a], Eirik Malinen[b,c], Linh Tran[d], Anatoly Rosenfeld[d], Marco Povoli[e], Angela Kok[e], Anand Summanwar[e], Dieter Röhrich[a]

[a] Department of Physics and Technology, University of Bergen, Norway
[b] Department of Physics, University of Oslo, Norway
[c] Department of Medical Physics, Oslo University Hospital, Norway
[d] Centre for Medical Radiation Physics, University of Wollongong, Australia
[e] SINTEF, Norway

ARTICLE INFO

Keywords:
Microdosimetry
Silicon-on-insulator
Beam quality
Radiobiology
Tissue equivalence

ABSTRACT

Introduction: An accurate description of the radiation quality of proton beams is a precondition to increase our understanding of radiobiological mechanisms and to develop accurate biological response models for radiotherapy. However, there are few detectors capable of measuring microdosimetric quantities with high spatial resolution along the entire Bragg curve due to the rapid increase in stopping power at the Bragg peak (BP) and distal dose fall-off (DDF). The aim of this work was to measure the microdosimetric spectra along the Bragg curve in a low energy proton beamline used for radiobiological experiments with a novel 3D silicon-on-insulator (SOI) "mushroom" microdosimeter.

Method: A silicon microdosimeter with an array of 3D structured diodes, creating well-defined sensitive volumes (SV) with excellent spatial resolution was used for microdosimetry. The microdosimeter was used to measure microdosimetric spectra and the relative dose throughout the Bragg curve of a 15 MeV proton beam by sequential insertion of 16 μm thick polyamide absorption films in front of the microdosimeter. The results were tissue corrected with a novel correction function and compared to Monte Carlo (MC) simulations performed in GATE.

Results: The measured dose-mean lineal energy ($\overline{y_D}$) increased from 8 keV/μm at the entrance to 24 keV/μm at the BP, rising to a maximum of 35 keV/μm at the DDF. The measured $\overline{y_D}$ showed an overall good agreement with the MC simulated values, with deviation of less than 2% at the BP and DDF, while the largest deviation (12%) was found at the entrance. Clear changes in microdosimetric spectra were seen for each 16 μm step at the BP and DDF.

Conclusion: The SOI microdosimeter with its well-defined 3D sensitive volumes is an excellent tool for characterizing low energy beamlines that demands very high spatial resolution. The good overall agreement between experimental and simulated results indicated that the detector is capable of accurate microdosimetric measurements.

1. Introduction

The biological effect of ionizing radiation depends on how the energy is deposited on a micrometric scale. This can be quantified by the linear energy transfer (LET) or through microdosimetry, and is often referred to as the radiation quality (ICRU, 1970, 1983). In a comprehensive review of the relative biological effectiveness (RBE) of protons as a function of LET in vitro, high variability was seen in the experimental results (Paganetti, 2014). The need to reduce uncertainties in proton RBE-models are also evident from a recent comparison of such models, as presented by (Rørvik et al., 2018). These uncertainties are likely to stem from both varying biological as well as experimental conditions, and it is of high importance to reduce the experimental uncertainties to accurately describe the action of ionizing radiation on living matter. The reported LET values in the data in Paganetti (2014) were not calculated in a consistent matter, and several radiobiological experiments did not report the LET. Thus, a generic Monte Carlo model of a proton therapy beamline was used to retrospectively calculate the

* Corresponding author.
E-mail address: andreas.samnoy@uib.no (A.T. Samnøy).

https://doi.org/10.1016/j.radphyschem.2020.109078
Received 25 February 2020; Received in revised form 1 June 2020; Accepted 23 June 2020
Available online 27 June 2020

LET in these cases. In order to reduce uncertainties, the beam quality should be determined precisely at the position of the cells in a radiobiological experiment to reduce the uncertainty of RBE as a function of beam quality, either through benchmarked LET calculations or by microdosimetric measurements. This can be achieved by using silicon microdosimeters.

The Centre of Medical Radiation Physics (CMRP), University of Wollongong, Australia, has developed and tested several generations of Silicon-on-Insulator (SOI) microdosimeters (Rosenfeld, 2016). The microdosimeters consists of an array of micrometer sized sensitive volumes (SV) embedded in a silicon chip and is an alternative to Tissue Equivalent Proportional Chambers (TEPC). The detector used in this study is the 5th and latest generation of SOI microdosimeters developed by CMRP and fabricated by SINTEF. The SVs were fabricated by forming true 3D cylindrical structures enclosed by a through substrate circular electrode (Rosenfeld, 2016) (Tran et al., 2018c). The array of SVs is connected in parallel and covers a 2.4 x 2.4 mm^2 area that is ~10 μm thick. This is considerably smaller than traditional TEPC which normally has diameters above 10 mm (Lindborg and Waker, 2017). The small size results in better spatial resolution and the ability to handle higher fluxes without suffering from pile-up. Due to the true micrometric volume of the SOI microdosimeter, they do not suffer from the wall effects that occur in walled TEPCs. The SOI microdosimeter is fully depleted and can be operated at 5 V and it does not require gas in the SV, and thus it generally easier to operate and requires fewer auxiliary systems. SOI microdosimeters are also cheap to mass produce once they are developed. However, the SOI microdosimeter is not tissue equivalent and the SV is relatively large compared to the gas-to-tissue mimicked volume in a TEPC, where the SOI microdosimeter chord length is approximately 10–15 μm, tenfold of typical TEPC sites. Similar detectors have been developed and characterized by (Fleta et al., 2015). Miniature TEPC has recently been developed to better address its application in a particle therapy (Conte et al., 2019).

The issue of tissue equivalence has been investigated previously (Rosenfeld, 2016; Bradley, 2000; Bradley and Rosenfeld, 1998; Bolst et al., 2017a; Agosteo et al., 2010), and a tissue correction factor has been used to transfer lineal energy spectra from silicon to tissue for typical energies in medical beamlines. However (Agosteo et al., 2010), showed that using a correction factor did not give satisfactory results for protons below 6.5 MeV when compared to a TEPC.

The primary aim of this work was to measure the microdosimetric spectra along the depth dose curve of a 15 MeV proton beamline used for radiobiological experiments. Moreover, a novel tissue correction function was introduced to increase the tissue correction accuracy for low energy protons. The setup is based on an established beamline used for radiobiological experiments, where a FLUKA based MC model has been used to estimate the beam quality through LET (Dahle et al., 2017). These MC simulations were benchmarked with dose measurements, but no microdosimetric measurements were performed. The results of this work serve as a microdosimetric characterization of the low energy proton beamline and as an evaluation of the novel tissue correction function.

2. Materials and methods

2.1. 3D SOI "mushroom" microdosimeters

The 3D SOI "mushroom" microdosimeter consists of a matrix of cylindrical diodes embedded in the silicon device layer, where the enclosed volume of the diodes defines the SV (Fig. 1). The energy lost by ionizing radiation through electron collisions in the SVs excites electrons into the conductive band before being collected at the central N+ electrode (red in Fig. 1). Thus, the amount of charge liberated in the SV is proportional to the energy deposited in the SV. The device active layer is 10 μm thick high resistivity p-type silicon. The diodes were fabricated using modern silicon sensor technology in combination with state-of-the-art micromachining. The key step to enclose the SVs was by etching a circular narrow trench through the entire device layer all the way down to the insulation layer of silicon dioxide. After the etching, the trenches were doped by Boron gas diffusion (p+) and the trenches were then filled with doped (p+) polysilicon for planarization. The N-electrode, where the bias is applied and the measured signal is collected, sits at the center of the diode surface. Since the diodes are enclosed by the 3-dimensional substrate trench P-electrode, no free charge generated outside the SV can be collected by the central N-electrode. This reduces cross talks and improves spatial resolution. The height and radius of the SVs were measured to be 9.1 and 15 μm respectively in (Tran et al., 2018c) using a scanning electron microscope. The microdosimeter chip has 33 x 33 SVs with a pitch of 75 μm in both directions, covering an area of 2.4 x 2.4 mm^2 where the odd and even columns of the SVs' central N-electrode are connected in parallel. Detailed description and charge collection studies of the detector can be found in (Tran et al., 2018c) where the detector design used in the current study here is termed "trenched planar structure".

2.2. Proton beam setup

The experiment was performed at the Oslo Cyclotron Laboratory (OCL) proton beam line, operated at an energy of approximately 15 MeV. The experiment was conducted in air at ~25°C and a schematic of the experimental setup is shown in Fig. 2, where the Beam Exit Window (BEW) is a 52 μm thick tungsten foil. To avoid pile-up and events during the detector dead-time, the beam intensity at the detector surface, 1 m from the BEW, was reduced by collimating the beam through a 1 mm hole and then scatter it through a 54 μm thick lead foil.

To monitor the beam intensity, a transmission chamber from PTW (Type 7862) was positioned 140 mm after the collimator and scattering foil and had 96.5 mm diameter window. The transmission chamber window consisted of four 50 μm thick polyimide films, and it was connected to an Unidos E Universal Dosemeter, also provided by PTW.

Polyamide (nylon6) absorber films with a density of 1.13 g/cm^3 were placed 890 mm from the BEW in a plastic frame with a 70 x 70 mm^2 opening. The films had a nominal thickness of 15 μm with 20% uncertainty according to the vendor. To minimize uncertainty in film thickness, 5 points were measured on all the films with both a Filmetrics F10-RT thin-film analyzer and a Mitutoyo Series 293 QuantuMike Micrometer. The resulting average film thickness was 16.4 μm, which is equivalent to 19.2 μm of water in the energy range of this experiment. The mean standard deviation from the 5 measured points on each film was 0.2 μm, indicating that there is little inhomogeneity across the film surfaces. The microdosimetric spectra were measured at 13 depths along the Bragg curve by sequential insertion of the polyamide films. At the BP and DDF, single sheets of a film were introduced between measurements to determine the change in microdosimetric spectra with high precision.

The microdosimeter was placed inside a steel box that served as both a light tight box and Faraday cage. The box had a 6 mm diameter hole in front of the detector for the beam to pass without absorption. The detector was connected to an Amptek A250CF CoolFET Charge Sensitive Preamplifier (CSP). The signal from the CSP was sent to a Tennelec 244 shaping amplifier set to 1 μs shaping time. Detector biasing was performed through the CSP by a Keithley 2635A SourceMeter and 20 V bias was applied. Signal testing was performed through the CSP with an Agilent/Keysight 33250A 80 MHz waveform generator. The signal output from the shaping amplifier was digitized by a SP Devices ADQ14 Analog to Digital Converter (ADC) with a PCI-Express interface to a computer. The digital signal was then filtered and the signal height and signal FWHM was recorded to a data file.

2.3. Monte Carlo simulations

In order to supplement and substantiate the experimental findings,

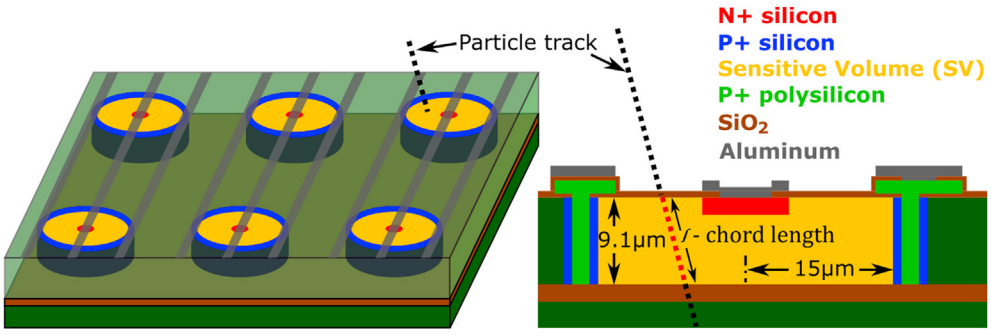

Fig. 1. Sketch of the 3D SOI "Mushroom" microdosimeter. The cylindrical diodes (yellow) make up the SVs of the microdosimeter and comprise the volume between the P+ circular trench (blue) and the central N+ electrode (red). The P+ circular trench that surrounds the SV extends all the way down to the silicon dioxide insulation layer and is filled with P+ polysilicon for planarization. The SV is thereby completely closed by the surrounding trenches and the insulation layer below. (For interpretation of the references to colour in this figure legend, the reader is referred to the Web version of this article.)

GEANT4 Monte Carlo simulation software (GATE v8.1) was used. The physics list QGSP_BIC_HP was applied for precise hadron and neutron calculations and the Livermore model (*emlivermore*) for precise electromagnetic calculations.

The simulation setup was identical to the experimental setup (Fig. 2). One simulation was run for every thickness of the polyamide absorber that was used in the experiment. For every event, the amount of energy lost in the microdosimeter SVs is recorded to file. The production cuts within 30 mm of the microdosimeter was 1 keV, while the production cuts in and around the SVs was 0.25 keV. The microdosimeter was also simulated as composed of tissue for comparison with the simulated silicon microdosimeter and the experimental results.

2.4. Microdosimetric quantities

The microdosimeter measures the deposited energy, ε_1, event by event. The lineal energy, y, of a single event is defined as (Rossi and Zaider, 1996; ICRU, 1983):

$$y = \frac{\varepsilon_1}{\bar{l}} \tag{1}$$

where $\bar{l}$ is the SV's mean cord length. Since the beam orientation is perpendicular onto the detector surface and due to the relative long distance between the absorbers and the detector, it is assumed that $\bar{l}$ is equal to the height of the SVs, 9.1 μm.

The probability density function of the lineal energy spectrum, $f(y)$, is derived from the energy deposition spectrum divided by $\bar{l}$. The dose weighted lineal energy distribution is given by

$$d(y) = \frac{yf(y)}{\overline{y_F}} \tag{2}$$

Where

$$\overline{y_F} = \int_0^\infty yf(y)dy \tag{3}$$

is the frequency-mean lineal energy, and the dose-mean lineal energy is given by

$$\overline{y_D} = \int_0^\infty yd(y)dy \tag{4}$$

The microdosimetric spectra are plotted as $yd(y)$ *vs* $\log(y)$, as is common practice in microdosimetry. Details on the fundamentals of microdosimetry and its quantities can be found in (Rossi and Zaider, 1996; ICRU, 1983).

2.5. Tissue correction

The microdosimetric spectra measured in this study has been corrected to tissue (muscle (skeletal) (ICRU, 1989);) to follow common practice in microdosimetry. As a new approach was developed and used in the current work, two other methods are revisited here for comparison. In (Bradley and Rosenfeld, 1998) the tissue equivalent energy deposition for a single ion, $\varepsilon_{1,T}$, was calculated by

$$\varepsilon_{1,T} = \varepsilon_{1,Si}\frac{1}{E_{max}}\int_0^{E_{max}}\frac{S_T(E)}{S_{Si}(E)}dE = \xi\cdot\varepsilon_{1,Si} \tag{5}$$

where S_T and S_{Si} is the stopping power for silicon and tissue respectively for ion energy E, while E_{max} is the maximum ion energy and $\varepsilon_{1,Si}$ is the single event energy deposition in the SV. ξ must be calculated for every present particle species and a weighted average of these is used to transfer to tissue equivalent energy deposition. This method has yielded good results for protons above 6.5 MeV when compared to a TEPC (Agosteo et al., 2010). However, since the stopping power ratio changes quickly below ~8 MeV (Rosenfeld, 2016) the correction produces larger errors at the BP and DDF, as shown by Agosteo et al. (2010).

As high energy ions generate a variety of secondary particles it is difficult to find the weighted average ξ. This is particularly challenging when estimating microdosimetric spectra along a Bragg curve, where the type, fraction and energies of the secondary particles change with depth. MC has in a previous study been used to calculate the lineal energy in silicon and tissue composed microdosimeters (Bolst et al., 2017a). In that work, the cylindrical SVs of the simulated silicon composed detector were modelled after the real detector, with equal height and radius, while the radius and height of a tissue composed SVs were $1/\kappa$ times larger. The aim was to find the correction factor, κ, giving approximately the same energy deposition in silicon and tissue at

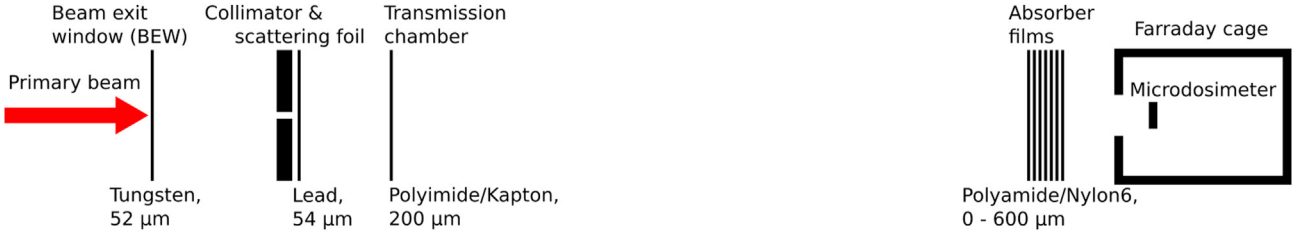

Fig. 2. Schematic of the experimental setup. Distance between beam exit window and the microdosimeter is 1 m. The thickness and material composition of all the objects is shown.

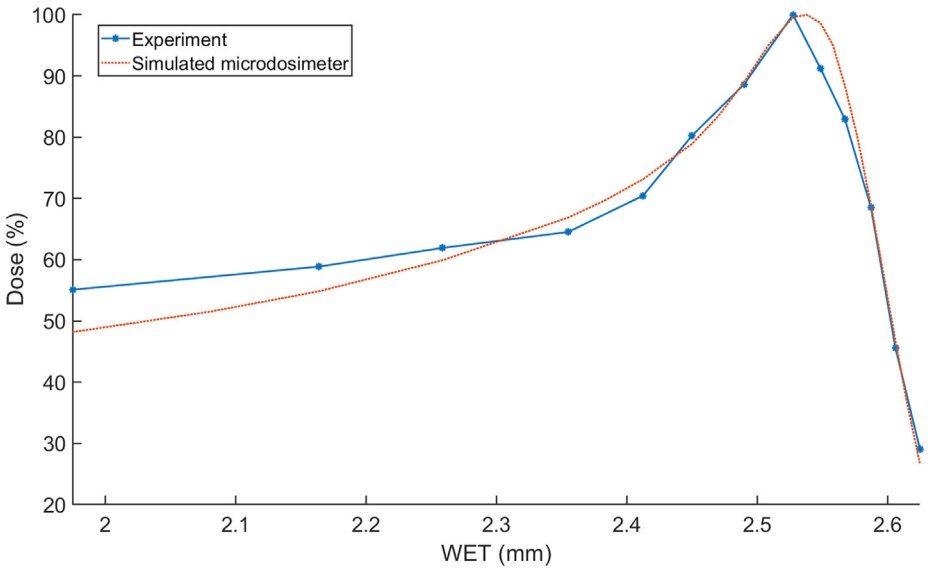

Fig. 3. Experimental and simulated depth dose distribution. The depicted simulated curve is for a 15.23 MeV proton beam with 0.04 MeV standard deviation and is the best fit to the experimental curve through the method of least squares. The x-axis starts at 1.98 mm WET, as this includes WETs of all objects apart from the absorbers, such as beam exit window, scattering foil, transmission chamber and 1 m of air (Fig. 2).

all depths of the Bragg curve, i.e. giving $\varepsilon_{1,Si} \approx \varepsilon_{1,T}$. The tissue equivalent lineal energy, y_T, is then

$$y_T = \frac{\overline{l_{Si}}}{\overline{l_T}} y_S = \kappa \cdot y_{Si} \tag{6}$$

where y_{Si} is the lineal energy to the silicon SV, while $\overline{l_{Si}}$ and $\overline{l_T}$ are the chord lengths in the silicon and tissue SVs respectively. Using this method, the best fitted κ was 0.57 for a 290 MeV/u ^{12}C beam in water (Bolst et al., 2017a). The study showed that $\kappa = 0.57$ yielded very good results except near the BP, where the tissue corrected $\overline{y_T}$ from the silicon detector was approximately 20% lower than that from a tissue composed SV, while $\overline{y_D}$ results were not shown. Other studies using this method has found that $\kappa = 0.58$ is the best fit in medical proton and ^{12}C beamlines as well as high energy ^{14}N and ^{16}O beamlines (Tran et al., 2017, 2018a, 2018b; Debrot et al., 2018; Bolst et al., 2017b). However, these studies did not show the relative difference between the simulated tissue corrected lineal energy from a silicon detector and that of a tissue composed detector which makes it difficult to assess the accuracy of the tissue correction factor.

By creating a tissue correction function that depends on the single event energy deposition within the silicon detector, $\kappa(\varepsilon_{1,Si})$, it is possible to convert the microdosimetric spectra to tissue equivalence more accurately than using a correction factor. In the current work, the tissue correction function for low energy protons was found by comparing the simulated energy deposition in a 9.1 μm high cylinder of silicon and 12.0, 12.5 and 13.0 μm high tissue cylinders from 0.725 to 200 MeV protons. The lower cutoff of 0.725 MeV was used since a significant fraction of the protons will stop within the detector at lower energies. The tissue and silicon composed cylinders were simulated in vacuum in the GATE software with a monoenergetic proton beam perpendicularly incident to the center of the cylinders. For each proton energy simulated, the ratio of the mean lineal energy to tissue over silicon was plotted against the mean energy deposited in the silicon detector, $\overline{y_T}/\overline{y_{Si}}$ *vs* $\overline{\varepsilon_{1,Si}}$. The resulting plot was fitted using cubic polynomial regression, and the resulting cubic function was used as an energy dependent tissue correction function $\kappa(\varepsilon_{1,Si})$. For each of the three simulated tissue thicknesses a correction function, $\kappa(\varepsilon_S)$, was generated. The error of the correction functions were estimated in the simulation of the experimental set up (Fig. 2) by comparing $\overline{y_D}$ from tissue composed microdosimeters with $\overline{y_D}$ from a silicon microdosimeter with the applied correction functions. The silicon microdosimeter had 9.1 μm high cylindrical SVs, while the tissue composed microdosimeters where simulated with 12.0, 12.5 and 13.0 μm high SVs. The radii of the SV where increased by the same factor as the height to preserve the shape of the SVs.

2.6. Depth dose and beam energy estimation

The relative depth dose distribution was determined from the microdosimetric measurements where the absorbed dose is proportional to the integral of the energy deposited from all the events. The highest measured count rate was 170 Hz, and the system had a 450 μs dead time after each event which were corrected for when calculating the relative dose. The integral dose at every point along the depth dose distribution was normalized by transmission chamber readings to account for fluctuations in beam intensity. The beam energy was initially set to 15 MeV in the simulations. To establish a more precise energy estimate, comparison between MC simulations and the experimental results of the relative depth dose distribution was used to adjust the simulated beam energy and energy spread. The method of least squares was used to determine the best fit. The best fit was found by stepping the simulated energy by 0.01 MeV, where each energy was simulated with multiple standard deviations separated by 0.02 MeV. The Water Equivalent Thickness (WET) and Water Equivalent Ratio (WER) were calculated for all materials in front of the detector and summed. The WET and WER for a material X were calculated by:

$$WER_X = \frac{\rho_X}{\rho_W}\frac{\bar{S}_X}{\bar{S}_W} \qquad \& \qquad WET_X = t_X * WER_X \tag{7}$$

Where ρ_X and ρ_W is the mass density of material X and water respectively; $\bar{S}_X$ and $\bar{S}_W$ is the mean mass stopping power for material X and water respectively, while t_X is the thickness of material X. The WET and WER for each object is calculated for the range of proton energies that passes though the specific material. The mean stopping power is therefore different for all the objects, as they will experience different proton energies. PSTAR data was used for calculating the mean stopping powers (Berger et al., 2017).

3. Results

Fig. 3 shows the measured and the simulated depth dose distribution that yielded best results to determine beam parameters through the method of least squares. This gave a mean proton beam energy of 15.23 MeV with 0.04 MeV standard deviation in energy just prior to the beam exit window, which then was used in all further simulations. The width of the beam prior to the collimator had no visible influence on

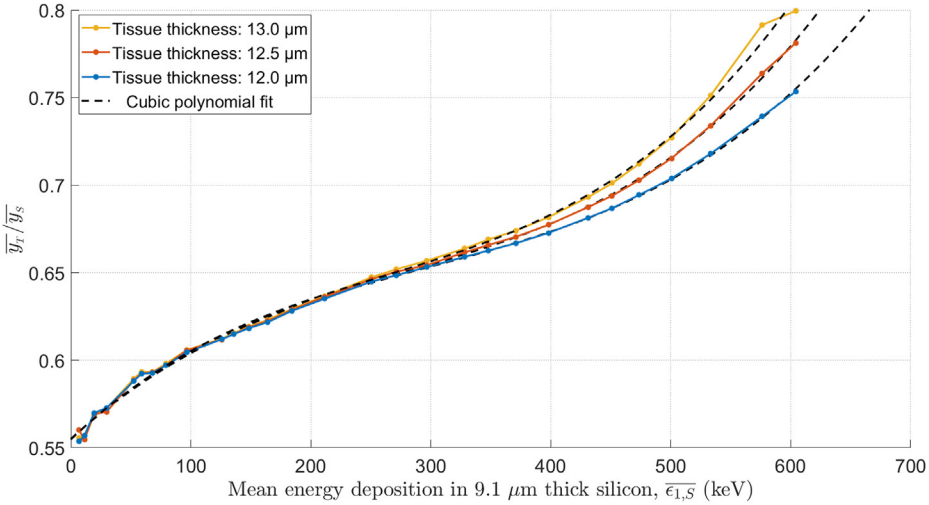

Fig. 4. Simulation results of $\overline{y_T}/\overline{y_S}$ from proton energies in the range 0.725 to 200 MeV from three different tissue thicknesses, where each data point indicate a specific proton energy incident on the simulated silicon and tissue SV.

the energy spectrum at the surface of the polyamide absorbers. The beam was therefore defined as a point source in all further simulations.

Fig. 4 shows the result of the novel tissue correction function for three different tissue thicknesses. For each simulated proton beam energy $\overline{y_T}/\overline{y_{Si}}$ is plotted against the mean deposited energy in the silicon detector, $\overline{\varepsilon_{1,Si}}$. Three tissue correction functions, $\kappa(\varepsilon_{1,Si})$, are made from the fitted cubic polynomials shown in Table 1. The tissue correction functions are restricted such that the maximum value for $\kappa(\varepsilon_{1,Si})$ is for 600 keV energy deposition, shown in the last column of Table 1.

The error estimation gave the least deviation in $\overline{y_D}$ between the 12.5 μm high tissue SVs and its respective transfer function, seen in Fig. 5. The tissue corrected $\overline{y_D}$ had a relative difference of -1.1% at the entrance and 0.4% at the DDF compared to the 12.5 μm high tissue composed SVs. Compared to the 12.0 μm high tissue SVs the relative difference at the entrance was -1.4% at the entrance and -3.1% at the DDF. For the 13.0 μm high tissue SVs the relative difference was -0.5% at the entrance and 4.2% at the DDF. By applying the method described in (Bolst et al., 2017a) in the current work, a tissue volume with 14.7 μm thickness ($\kappa = 0.62$) would yield excellent results at the entrance, but much worse in the DDF with relative difference of -11% for $\overline{y_D}$, as seen in Fig. 5.

Fig. 6 shows a comparison of experimental and simulated microdosimetric spectra at four depth, where the experimental results has been converted to tissue equivalence through the function $\kappa(\varepsilon_{1,S})$ and the simulated detector is composed of tissue with 12.5 μm high SVs. The microdosimetric spectra shown are from the entrance (1.98 mm WET), just prior to the BP (2.41 mm WET), approximately at the BP (2.53 mm WET) and at approximately 50% of dose max in the DDF (50%DDF) (2.61 mm WET). These positions are also marked in Fig. 7 that show $\overline{y_D}$ at all depths of the experiment.

The microdosimetric spectra at the entrance and prior to BP are Gaussian like, and the experimental results show a slightly higher mean and slightly wider distribution than the simulation. At the BP and 50% DDF, the shape and position of the experimental and simulated spectra matches very well, although the experimental spectra are slightly wider, with the falling edge slightly shifted towards higher lineal energy. At the entrance, the majority of the events (full width at 5% of maximum d(y)) were between 4.1 and 10.5 keV/μm, while prior to the BP they ranged from 7.6 to 21 keV/μm, although events up to 65 keV/μm were registered at both these positions. At the BP, the majority of events were between 9.5 and 60 keV/μm, while at 50%DDF the range was 12 to 61 keV/μm.

The experimental and simulated dose-mean lineal energy, $\overline{y_D}$, at all depths is shown in Fig. 7. The measured tissue equivalent $\overline{y_D}$ was 8.0 keV/μm at the entrance, approximately 13 keV/μm just prior to the BP, and reached 24 keV/μm at BP before rising to highest measured $\overline{y_D}$ in the DDF of 35 keV/μm. The overall shape of the measured curve matches well with the simulated tissue composed microdosimeter. The largest difference between the experiment and simulation is observed at the entrance with a 12% relative difference and 0.9 keV/μm absolute difference. At the BP the relative difference was 2% and in the DDF the deviation was less than 1%.

Fig. 8 shows all the 13 recorded microdosimetric spectra along the Bragg curve, where the binning increases with depth to make them readable as count rate decreases and spectrum width generally increases with depth. The depth between the last 6 spectra are separated by single polyamide films, approximately 19 μm WET and the rising edge of all spectra are clearly distinguishable. At the BP (2.527 mm) and in the DDF the falling edges of the spectra are almost equal at approximately 60 keV/μm, which corresponds to the proton energy of exact stoppers in silicon.

Table 1
Coefficients for the three cubic regression fits shown in Fig. 4. The cubic functions are used as tissue correction functions, $\kappa(\varepsilon_{1,S}) = a\varepsilon_{1,S}^3 + b\varepsilon_{1,S}^2 + c\varepsilon_{1,S} + d$, where $\varepsilon_{1,S}$ is the energy deposited in the silicon detector given in keV. The last columns show the maximum permitted value for $\kappa(\varepsilon_{1,S})$ when the energy deposition is above 600 keV.

Tissue thickness (μm)	a (keV^{-3})	b (keV^{-2})	c (keV)	D	$\kappa(\varepsilon_{1,S} > 600$ keV)
12.0	1.619E-09	-1.454E-06	6.183E-04	0.555	0.752
12.5	1.933E-09	-1.600E-06	6.386E-04	0.555	0.779
13.0	2.156E-09	-1.691E-06	6.525E-04	0.555	0.803

4. Discussion

The novel 3D SOI "mushroom" microdosimeter was used to measure the microdosimetric spectra along the Bragg curve in a low energy proton beamline. The experiment demonstrated the excellent spatial resolution of the microdosimeter. The results showed reasonable agreement with GATE/GEANT4 MC simulations in the entrance and plateau region, and very good agreement at the BP and the DDF.

Previous studies with similar silicon microdosimeters have used constant tissue correction factors in medical proton and ^{12}C beamlines as well as high energy ^{14}N and ^{16}O beamlines with $\kappa = 0.58$ (Tran et al., 2017, 2018a, 2018b; Debrot et al., 2018; Bolst et al., 2017b). Although several of these studies compare the experimental results with MC

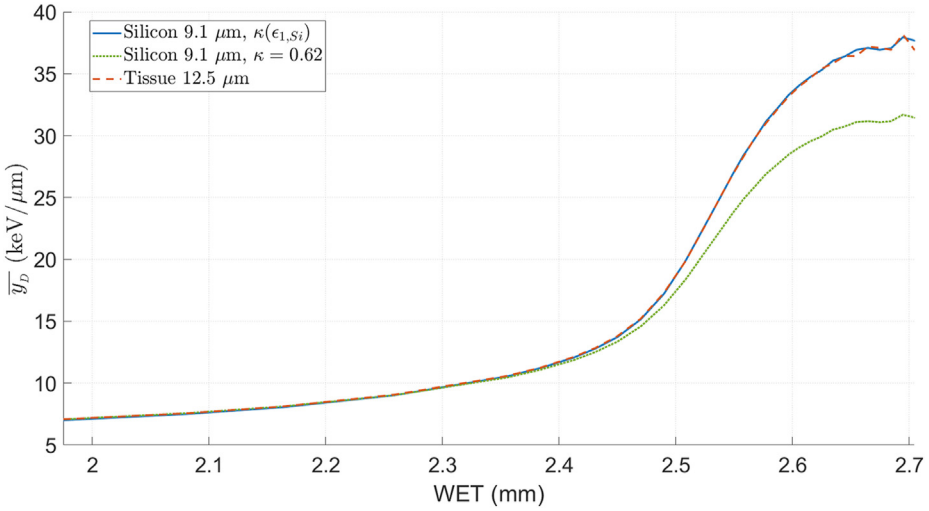

Fig. 5. Simulated dose-mean lineal energy at all depths of the experiment by a tissue-composed detector with 12.5 high cylindrical SVs (red) and a silicon detector with 9.1 μm high cylindrical SVs where the lineal energy has been tissue corrected with the function $\kappa(\varepsilon_{1,S})$ (blue) and a the factor $\kappa = 0.62$ (green). (For interpretation of the references to colour in this figure legend, the reader is referred to the Web version of this article.)

simulations, they are compared with a simulation of a silicon and not a tissue composed microdosimeter. The method for establishing the tissue correction factor $\kappa = 0.58$ in the above mentioned work is described in (Bolst et al., 2017a), where microdosimetric spectra from a medical ^{12}C of silicon, water and tissue composed SV are simulated and compared. The study shows that the use of $\kappa = 0.58$ yield very good results except near the BP. At the BP the tissue corrected $\overline{y_F}$ from the silicon detector is approximately 20% lower than that from a tissue composed SV, while $\overline{y_D}$ is not shown. Agosteo et al. (2010) measured the microdosimetric spectra from a 62 MeV SOBP proton beam with a ΔE/E two stage detector, where the protons were measured in both a 2 μm thick silicon (ΔE) and a 500 μm thick silicon (E). As protons below 6.5 MeV stopped completely inside the E stage of the detector, the tissue correction factor could be calculated as the stopping power ratio of tissue and silicon for the exact energy. For protons above 6.5 MeV, a constant $\kappa = 0.574$ was used. The results were compared to that of a TEPC and showed good agreement for $\kappa = 0.574$ above 6.5 MeV and for variable κ below 6.5 MeV. However, the agreement was not good when $\kappa = 0.574$ was used for proton energies below 6.5 MeV.

As the current work was conducted with a single stage detector, it was not possible to adjust the tissue correction based on proton energy, and a tissue correction function that was based on the energy deposition in the SV was developed. By simulating both a silicon and tissue composed microdosimeter in the experimental setup, it was shown that the tissue correction function significantly reduced the error compared to a constant tissue correction factor. For proton energies between 200 and 7 MeV, the correction function will vary between 0.56 and 0.60, which is similar to the work mentioned above. However, the correction function increased to a maximum of 0.78 for 0.725 MeV protons. Although the tissue correction function gave a smaller error compared to the best-fitted constant, some issues are still present. The correction function will not be equal for all secondary particles which causes erroneous correction for the secondary particles. This will become an increasing problem at higher energies and with heavier primary particles, as this will produce more secondaries with higher energies and a larger variation in types of secondary particles. However, for electrons that will deposit energies from a few keV up to a few tens of keV the correction function will vary between 0.56 and 0.58, which is also similar to the correction factor used in the work mentioned above. It is thus expected that the correction function would yield similar results in the entrance and plateau region of a medical proton beamline compared to a constant but would give better results in the BP and the DDF.

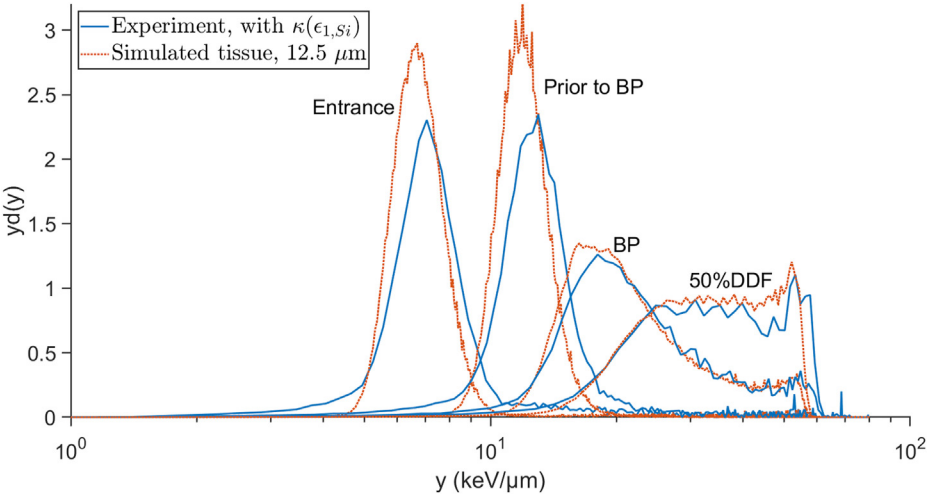

Fig. 6. Comparison of microdosimetric spectra from experiment and simulated tissue composed microdosimeter at 4 depths; entrance, prior to the BP, at BP and 50% DDF. The experimental results have been converted to tissue equivalence through the function $\kappa(\varepsilon_{1,S})$.

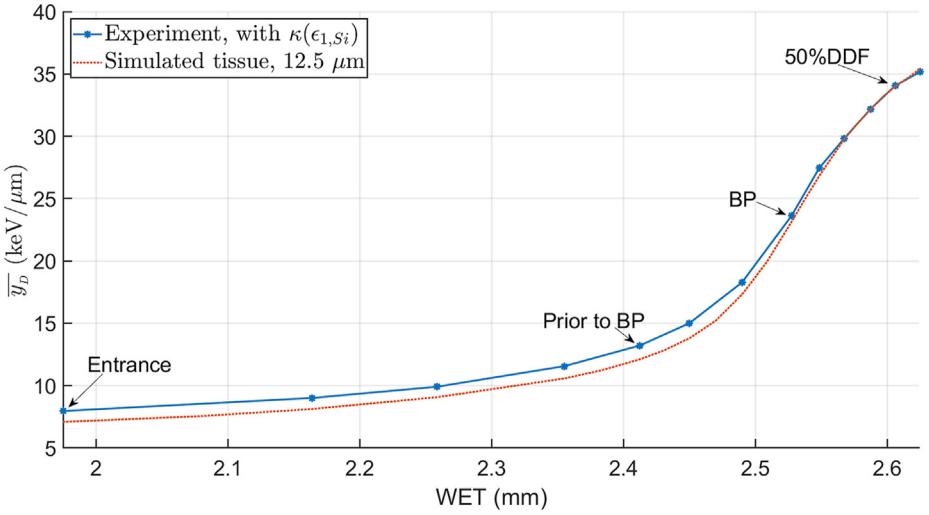

Fig. 7. Comparison of $\overline{y_D}$ at all depths from the experiment and simulated tissue composed microdosimeter. The experimental results have been converted to tissue equivalence through the function $\kappa(\varepsilon_{1,S})$, and the simulated results are from a tissue composed microdosimeter with 12.5 μm high SVs.

Another issue with the correction function is that it will slightly broaden the lineal energy spectra compared to a true tissue equivalent SV. When two identical particles with the same energy and direction deposit energy in a true tissue equivalent SV they will deposit unequal amounts of energy due to the stochastic nature of energy deposition. When the same two particles deposit energy in a silicon SV the same stochastics nature will lead to two different energy depositions as well. However, when the energy deposition in silicon is converted to its equivalent in tissue, the smaller energy deposition will be multiplied with a smaller $\kappa(\varepsilon_S)$, while the larger event is multiplied with a larger $\kappa(\varepsilon_S)$. This leads to a broadening, where the spectrum from a silicon microdosimeter corrected to tissue equivalence by $\kappa(\varepsilon_S)$ is slightly broader than the spectrum from a true tissue equivalent microdosimeter.

The measured and simulated microdosimetric spectra and $\overline{y_D}$ show excellent agreement at the BP and DDF with less than 2% deviation. The largest deviation is seen at the entrance with a 12% difference in $\overline{y_D}$ and a slightly wider distribution. This deviation is believed to come mainly from inaccurate initial beam parameters in the simulation. Although the number of $\overline{y_D}$ events above 20 keV/μm are very few, they occurred much more frequent in the experiment than in the simulation. This gives reason to believe that the beam had a higher amount of low energy protons than were simulated. If all events with $\overline{y_D}$ above 20 keV/μm at the entrance are removed from simulation and experimental results, then the deviation is reduced to 5.7%. Similarly, the relative difference in peak position in the experiment and simulation at the entrance is approximately 6%. Low energy protons would therefore explain difference in the spectra at the entrance, but as they would be stopped in the absorbers at greater depth, they would have little to no impact at the BP and DDF. This is consistent with the measured depth dose distribution (Fig. 3) being higher than the simulated at the entrance, as the low energy protons would deposit a higher dose than the

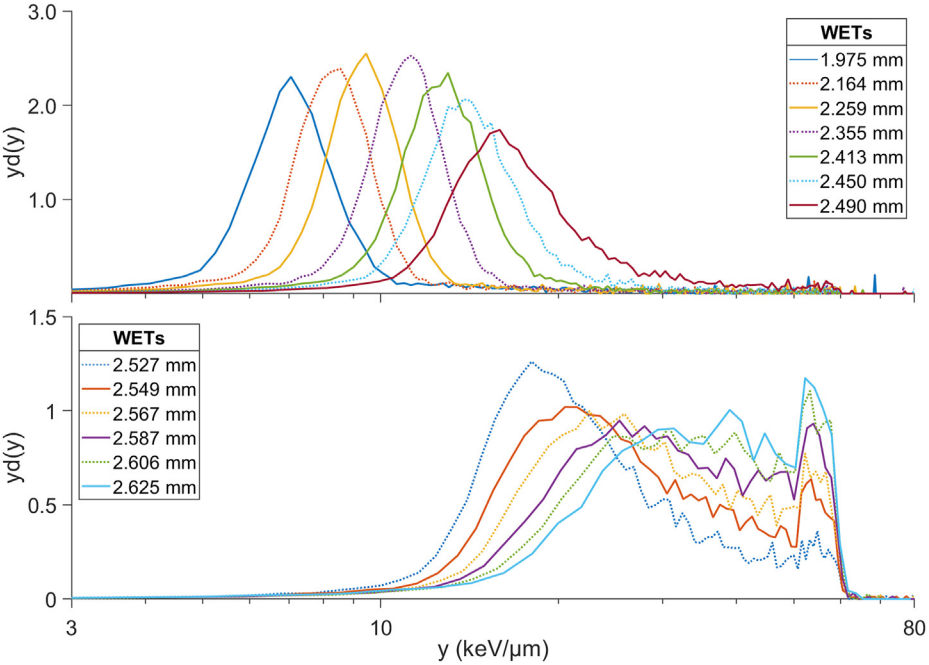

Fig. 8. All the 13 experimental microdosimetric spectra along the Bragg curve. The 7 first at top, and 6 last at bottom. The legend gives the depth in water equivalent thickness (WET).

more energetic ones.

While the experimental and simulated $\overline{y_D}$ matched well at BP and in the DDF, the microdosimetric spectra (Fig. 6) showed that the falling edge of the corrected experimental result was at slightly higher y values than the simulation. The falling edge would be at approximately equal y values if the transfer function for 12.0 μm tissue were used instead of the 12.5 μm. This is because the energy that gives exactly 9.1 μm proton path lengths in silicon also gives 12.0 μm path lengths in tissue according to GATE simulations. However, using the 12.0 μm tissue correction function would result in larger errors for $\overline{y_D}$.

The results show that the low energy proton beam produces lineal energy spectra with $\overline{y_D}$ ranging from 8 to 35 keV/μm, which is much higher than what is achievable in a medical beamline with similarly sized SVs due to range straggling. The microdosimetric spectra at each 19 μm WET step is clearly distinguishable from each other, even at the BP and DDF. This demonstrates the excellent spatial resolution obtainable with these microdosimeters. Microdosimetric measurements using a similar microdosimeter of a 131 MeV medical proton pencil beam (Tran et al., 2017) showed that the range of $\overline{y_D}$ in a was approximately 2 to 10 keV/μm. Thus, the low energy proton beamline used in the current work is excellent for establishing if the RBE as a function of $\overline{y_D}$ is the same for different particle species, as low energy protons produces lineal energy in the same range as higher energies of e.g. helium and carbon ions.

The $\overline{y_D}$ distribution along the Bragg curve in Fig. 7 shows that $\overline{y_D}$ changes rapidly with depth around the BP. The increase of $\overline{y_D}$ around BP is approximately 0.15 keV/μm per μm of water. This shows the sensitivity of such experiments and simulations to initial beam parameters, absorber thicknesses and other uncertainties in the experimental setup, and illustrates how small errors can give rise to large systemic uncertainties in $\overline{y_D}$ and LET. This could explain some of the large variability in previously published experimental proton RBE as a function of beam quality, as discussed by Paganetti (2014). With inexpensive and accurate measuring tools as presented here, this uncertainty may be reduced.

5. Conclusion

The novel 3D SOI “mushroom” microdosimeter was used to record microdosimetric spectra along the Bragg curve of a low energy proton beam used for radiobiological experiments. A tissue correction function, $\kappa(\varepsilon_S)$, was developed to transfer the measured lineal energy to tissue equivalence. The function was shown to give significantly less error than a correction factor coefficient at the end of the proton tracks in the current experiment.

Measured values of $\overline{y_D}$ ranged from 8 keV/μm at the entrance to 35 keV/μm in the DDF. The recorded spectra match well with simulation results in both shape and mean value, with less than 2% deviation in $\overline{y_D}$ at the BP and DDF. The largest relative difference was 12% at the entrance, corresponding to an absolute difference of 0.9 keV/μm, which is believed to stem from an underestimation of low energy protons in the simulation.

At the BP and DDF single sheets of absorbers with approximately 19 μm WET were inserted between measurement and a clear change in the recorded microdosimetric spectra can be seen. This demonstrates the capability of 3D SOI “mushroom” microdosimeter to accurately measure microdosimetric spectra with ultra-high spatial resolution. Such measurements can reduce the uncertainty in beam quality of radiobiological experiment and thereby contribute to better understanding and more accurate modelling of biological effects and their variations with beam quality.

Funding

This work was supported by the Research Council of Norway via the NANO2021 program.

CRediT authorship contribution statement

Andreas Tefre Samnøy: Conceptualization, Methodology, Formal analysis, Investigation, Writing - original draft, Writing - review & editing. **Kristian S. Ytre-Hauge:** Conceptualization, Methodology, Resources, Writing - review & editing, Supervision, Funding acquisition. **Eirik Malinen:** Resources, Writing - review & editing. **Linh Tran:** Resources, Writing - review & editing. **Anatoly Rosenfeld:** Resources, Writing - review & editing. **Marco Povoli:** Resources, Writing - review & editing. **Angela Kok:** Resources, Writing - review & editing. **Anand Summanwar:** Resources, Writing - review & editing. **Dieter Röhrich:** Resources, Writing - review & editing, Supervision, Funding acquisition.

Declaration of competing interest

The authors declare that they have no known competing financial interests or personal relationships that could have appeared to influence the work reported in this paper.

Acknowledgment

The authors would like to thank Dr. M. M. Greve at the department of physics and technology at UiB for his help in measuring the thickness of the polyamide absorber films, and the people at OCL for all the help during the experiment. The authors would also like to thank all collaborators in the 3DMiMic collaboration.

References

Agosteo, S., Cirrone, G.A.P., Colautti, P., Cuttone, G., D'Angelo, G., Fazzi, A., Introini, M.V., Moro, D., Pola, A., Varoli, V., 2010. Study of a Silicon telescope for solid state microdosimetry: Preliminary measurements at the therapeutic proton beam line of CATANA. Radiat. Meas., vol. 45, 1284–1289.

Berger, M.J., Coursey, J.S., Zucker, M.A., Chang, J., 2017. Stopping-Power & Range Tables for Electrons, Protons, and Helium Ions. National Institute of Standards and Technology.

Bolst, D., Guatelli, S., Tran, L.T., Chartier, L., Lerch, M.L., Matsufuji, N., Rosenfeld, A.B., 2017a. Correction factors to convert microdosimetry measurements in silicon to tissue in (12)C ion therapy. Phys. Med. Biol. 62, 2055–2069.

Bolst, D., Tran, L.T., Chartier, L., Prokopovich, D.A., Pogossov, A., Guatelli, S., Reinhard, M.I., Petasecca, M., Lerch, M.L.F., Matsufuji, N., Perevertaylo, V.L., Fleta, C., Pellegrini, G., Jackson, M., Rosenfeld, A.B., 2017b. RBE study using solid state microdosimetry in heavy ion therapy. Radiat. Meas. 106, 512–518.

Bradley, P.D., 2000. The Development of a Novel Silicon Microdosimeter for High LET Radiation Therapy. University of Wollongong).

Bradley, P.D., Rosenfeld, A.B., 1998. Tissue equivalence correction for silicon microdosimetry detectors in boron neutron capture therapy. Med. Phys. 25, 2220–2225.

Conte, V., Bianchi, A., Selva, A., Petringa, G., Cirrone, G.A.P., Parisi, A., Vanhavere, F., Colautti, P., 2019. Microdosimetry at the CATANA 62 MeV proton beam with a sealed miniaturized TEPC. Phys. Med., vol. 64, 114–122.

Dahle, T.J., Rykkelid, A.M., Stokkevåg, C.H., Mairani, A., Görgen, A., Edin, N.J., Rørvik, E., Fjæra, L.F., Malinen, E., Ytre-Hauge, K.S., 2017. Monte Carlo simulations of a low energy proton beamline for radiobiological experiments. Acta Oncol. 56, 779–786.

Debrot, E., Tran, L., Chartier, L., Bolst, D., Guatelli, S., Vandevoorde, C., Kock, E d, Beukes, P., Symons, J., Nieto-Camero, J., Prokopovich, D.A., Chiriotti, S., Parisi, A., Saint-Hubert, M.D., Vanhavere, F., Slabbert, J., Rosenfeld, A.B., 2018. SOI microdosimetry and modified MKM for evaluation of relative biological effectiveness for a passive proton therapy radiation field. Phys. Med. Biol. 63, 235007.

Fleta, C., Esteban, S., Baselga, M., Quirion, D., Pellegrini, G., Guardiola, C., Cortés-Giraldo, M.A., López, J.G., Ramos, M.C.J., Gómez, F., Lozano, M., 2015. 3D cylindrical silicon microdosimeters: Fabrication, simulation and charge collection study. J. Instrum. 10 P10001-P.

ICRU, 1970. Linear energy transfer. In: Report 16: International Commission on Radiation Units and Measurements.

ICRU, 1983. Microdosimetry. In: Report 36: International Commission in Radiation Units and Measurements.

ICRU, 1989. Tissue substitutes in radiation dosimetry and measurement. In: Report 44: International Commission in Radiation Units and Measurements.

Lindborg, L., Waker, A., 2017. Microdosimetry: Experimental Methods and Applications. CRC Press.

Paganetti, H., 2014. Relative biological effectiveness (RBE) values for proton beam therapy. Variations as a function of biological endpoint, dose, and linear energy transfer. Phys. Med. Biol. 59, R419–R472.

Rosenfeld, A.B., 2016. Novel detectors for silicon based microdosimetry, their concepts and applications. Nucl. Instrum. Methods Phys. Res. Sect. A Accel. Spectrom. Detect.

Assoc. Equip. 809, 156–170.
Rossi, H.H., Zaider, M., 1996. Microdosimetry and its Applications. Springer.
Rørvik, E., Fjæra, L.F., Dahle, T.J., Dale, J.E., Engeseth, G.M., Stokkevåg, C.H., Thörnqvist, S., Ytre-Hauge, K.S., 2018. Exploration and application of phenomenological RBE models for proton therapy. Phys. Med. Biol. 63, 185013.
Tran, L.T., Bolst, D., Guatelli, S., Pogossov, A., Petasecca, M., Lerch, M.L.F., Chartier, L., Prokopovich, D.A., Reinhard, M.I., Povoli, M., Kok, A., Perevertaylo, V.L., Matsufuji, N., Kanai, T., Jackson, M., Rosenfeld, A.B., 2018a. The relative biological effectiveness for carbon, nitrogen, and oxygen ion beams using passive and scanning techniques evaluated with fully 3D silicon microdosimeters. Med. Phys. 45, 2299–2308.
Tran, L.T., Chartier, L., Bolst, D., Davis, J., Prokopovich, D.A., Pogossov, A., Guatelli, S., Reinhard, M.I., Petasecca, M., Lerch, M.L.F., Matsufuji, N., Povoli, M., Summanwar, A., Kok, A., Jackson, M., Rosenfeld, A.B., 2018b. In-field and out-of-file application in 12C ion therapy using fully 3D silicon microdosimeters. Radiat. Meas. 115, 55–59.
Tran, L.T., Chartier, L., Bolst, D., Pogossov, A., Guatelli, S., Petasecca, M., Lerch, M.L.F., Prokopovich, D.A., Reinhard, M.I., Clasie, B., Depauw, N., Kooy, H., Flanz, J.B., McNamara, A., Paganetti, H., Beltran, C., Furutani, K., Perevertaylo, V.L., Jackson, M., Rosenfeld, A.B., 2017. Characterization of proton pencil beam scanning and passive beam using a high spatial resolution solid-state microdosimeter. Med. Phys. 44, 6085–6095.
Tran, L.T., Chartier, L., Prokopovich, D.A., Bolst, D., Povoli, M., Summanwar, A., Kok, A., Pogossov, A., Petasecca, M., Guatelli, S., Reinhard, M.I., Lerch, M., Nancarrow, M., Matsufuji, N., Jackson, M., Rosenfeld, A.B., 2018c. Thin silicon microdosimeter utilizing 3-D MEMS fabrication technology: charge collection study and its application in mixed radiation fields. IEEE Trans. Nucl. Sci. 65, 467–472.